

Monte Carlo simulations of crystal defects in open ensembles

Flynn Walsh, Babak Sadigh, Joseph T. McKeown, and Timofey Frolov
Lawrence Livermore National Laboratory, Livermore, California 94550, USA

Open materials systems are often inaccessible to conventional atomistic simulations, which add and remove atoms by creating high-energy defects that may be sampled with vanishing probability. This longstanding challenge motivates a new Hamiltonian Monte Carlo method that maps the grand canonical problem to a canonical system involving non-interacting fictitious particles. To trial deletions or insertions, a real or fictitious particle is selected according to an energy-based biasing scheme and gradually transformed over a microcanonical molecular dynamics trajectory. The method is validated, optimized, and used to compute point defect free energies that allow for arbitrary structures and interactions among multiple defects. Several grain boundaries are then equilibrated in a physically representative open ensemble, demonstrating a new approach to studying interface structures and their phase transitions.

I. INTRODUCTION

Many physical systems can be modeled as open statistical ensembles containing variable numbers of particles (N) that are exchanged with reservoirs of constant chemical potential (μ). In crystals, open ensembles naturally describe point defects and grain boundaries (GBs), which form distinct structures for different values of N with consequences for macroscale properties [1–5]. The grand canonical (μVT) ensemble, which fixes volume (V) and temperature (T) in addition to μ , receives the most attention, but solids usually experience fixed pressure (P) rather than volume. This reality motivates the μPT ensemble [6, 7], which, though not appropriate for macroscopic systems, can represent atomic scale solids within a region of convex free energy [8].

As in any other ensemble, μPT and μVT properties can be calculated by Monte Carlo (MC) sampling. Standard Markov chain MC constructs a series of microstates by iteratively trialing mutations that are accepted with probability reproducing the desired energetic distribution. The simplest way to mutate N is by randomly adding and removing particles, which, as a reversible procedure, can guarantee correctness by satisfying the condition of detailed balance. In dense solids and liquids, however, naively adding or removing particles creates high-energy defects that are typically sampled with very low probability. Some degree of structural relaxation is required to generate insertion and deletion trials that will be accepted at practical rates, but energy optimization is generally irreversible and therefore not well motivated.

Directly jumping among distinct structures may be possible in certain situations, but constructing these moves requires significant effort in practice [9]. As another approach, equilibrium molecular dynamics (MD) simulations can gradually add and remove particles by integrating atomic fractions as an additional degree of freedom with corresponding equations of motion [10–13]. Similar techniques have been employed within MC frameworks [14, 15], but the presence of unphysical partial particles is less than desirable in both cases. In solids, this

approach has been primarily considered for structure optimization rather than thermodynamics [2].

However, the promise of gradual insertions and deletions via MD can be fully realized using the flexibility of MC sampling, which permits any moves that satisfy statistical balance. For instance, in canonical (NVT) MC simulations, deterministic and reversible microcanonical (NVE) MD can generate trial states with probabilities corresponding to the choice of initial velocities. This technique, which is known as Hamiltonian or hybrid MC [16, 17], can also sample non-physical trajectories. For example, the addition of a fourth-dimension has been used to move pair-interacting particles between a liquid and explicit reservoir [18, 19].

This work explores the addition and removal of solid atoms through the trajectories of a time-dependent Hamiltonian. Atoms are not truly created or destroyed, but exchanged with a non-interacting gas of fictitious particles in a canonical representation of the grand canonical problem. Specific particle transformations are attempted with a bias toward deleting high-energy atoms and inserting fictitious particles with low hypothetical energies. Together, these techniques enable practical, general, and rigorous simulations of dense solids with variable numbers of atoms. After validation and optimization, the method is used to calculate the complete free energies of point defects, which fully account for non-ideal configurational entropy. The remainder of the study examines several crystal GBs, which are successfully equilibrated at different temperatures and chemical potentials.

II. RESULTS

A. Canonical representation

A classical μVT system consists of variable N particles with positions \mathbf{x}^N , momenta $m\mathbf{v}^N$, and potential energy $U(\mathbf{x}^N)$. The kinetic component of the partition function analytically integrates to $\Lambda^{-3N} = (2\pi m/\beta h^2)^{3N/2}$ when combined with the normalization factor of Planck's constant, where $\beta = (k_B T)^{-1}$. The partition function then

simplifies to

$$Z = \sum_{N=0}^{\infty} \frac{1}{N!} \frac{1}{\Lambda^{3N}} \int d\mathbf{x}^N e^{-\beta(U(\mathbf{x}^N) - \mu N)}. \quad (1)$$

To compute ensemble properties, the sum of integrals in Eq. (1) can be approximated by sampling a collection of microstates with relative probabilities

$$\pi(\mathbf{x}^N) \propto \frac{1}{N!} \frac{1}{\Lambda^{3N}} e^{-\beta(U(\mathbf{x}^N) - \mu N)}. \quad (2)$$

In practice, drawing microstates from an equivalent canonical ensemble can be more convenient. As long as all states with $N > M$ have negligible probability, then an M -particle system of N real and $M - N$ fictitious particles can fully represent the problem [20]. The additional fictitious particles should not interact with real particles or each other such that the real subsystem, $\mathbf{x}^{N \subset M}$, determines the potential energy of M -particle microstates, i.e. $U(\mathbf{x}^M) = U(\mathbf{x}^{N \subset M})$.

A system of M particles contains many copies of each N -particle microstate, corresponding to all the different ways to have choose N real particles from M total. Accounting for all $\binom{M}{N}$ possibilities, sampling the M -particle system with arbitrary probability $\pi'(\mathbf{x}^M) = \pi'(\mathbf{x}^{N \subset M}) \neq \pi(\mathbf{x}^N)$ approximates the expression

$$\sum_{N=0}^M \frac{M!}{N!(M-N)!} \int d\mathbf{x}^M \pi'(\mathbf{x}^{N \subset M}). \quad (3)$$

Since the sampled distribution depends only on the real subsystem, the integrals over fictitious coordinates simplify as $\int d\mathbf{x}^{M-N} = V^{M-N}$. Then, sampling the M -particle system of Eq. (3) with

$$\pi'(\mathbf{x}^{N \subset M}) = \frac{(M-N)!}{M!} \frac{V^{N-M}}{\Lambda^{3N}} e^{-\beta(U(\mathbf{x}^{N \subset M}) - \mu N)} \quad (4)$$

recovers the grand canonical integral of Eq. (1) as

$$\sum_{N=0}^M \frac{1}{N!} \frac{1}{\Lambda^{3N}} \int d\mathbf{x}^N e^{-\beta(U(\mathbf{x}^{N \subset M}) - \mu N)}. \quad (5)$$

B. Monte Carlo sampling

Markov chain MC samples an ensemble by drawing microstates with probabilities that depend only on the immediately prior state. That is, the probability of transitioning from microstate \mathbf{x}_a to microstate \mathbf{x}_b is some constant K_{ab} . Accordingly, the probability of sampling \mathbf{x}_b relates to the probability of preceding \mathbf{x}_a as $\pi(\mathbf{x}_b) = \int d\mathbf{x}_a \pi(\mathbf{x}_a) K_{ab}$. This condition enables the determination of transition probabilities, which are more easily found by imposing the sufficient though stricter requirement of detailed balance,

$$\pi(\mathbf{x}_a) K_{ab} = \pi(\mathbf{x}_b) K_{ba}, \quad (6)$$

as $\int d\mathbf{x}_a K_{ba} = 1$ for any \mathbf{x}_b . Eq. (6) specifically requires that all moves between \mathbf{x}_a and \mathbf{x}_b are reversible with quantifiable probability, which precludes any structure optimization that moves downhill in the potential energy landscape.

Transitions are performed by trialing candidate states drawn from some fixed distribution, W_{ab} . Trials are accepted with probability A_{ab} to achieve transition rates $K_{ab} = W_{ab} A_{ab}$ that satisfy Eq. (6), specifically

$$A_{ab} = \min \left(1, \frac{W_{ba} \pi(\mathbf{x}_b)}{W_{ab} \pi(\mathbf{x}_a)} \right). \quad (7)$$

From Eq. (4), the microstate probability ratios in deletion and insertion trials are, respectively,

$$\frac{\pi'(\mathbf{x}_b^{N-1 \subset M})}{\pi'(\mathbf{x}_a^{N \subset M})} = \frac{M-N+1}{V \Lambda^{-3}} e^{-\beta(U(\mathbf{x}_b^{N-1 \subset M}) - U(\mathbf{x}_a^{N \subset M}) + \mu)}, \quad (8)$$

$$\frac{\pi'(\mathbf{x}_b^{N+1 \subset M})}{\pi'(\mathbf{x}_a^{N \subset M})} = \frac{V \Lambda^{-3}}{M-N} e^{-\beta(U(\mathbf{x}_b^{N+1 \subset M}) - U(\mathbf{x}_a^{N \subset M}) - \mu)}. \quad (9)$$

The other half of Eq. (7) depends on trial probability densities W_{ab} and W_{ba} , which are the composite of several steps. First, the type of MC is chosen: displacements, deletions, and insertions were respectively attempted with probabilities W^0 , W^- , and W^+ . Deletions and insertions also select a particle for gradual transformation. Most simply, random $W_a^{-i} = 1/N$ and $W_a^{+i} = 1/(M-N)$, but more efficient choices are examined later. Finally, Verlet integration evolved the system from \mathbf{x}_a to \mathbf{x}_b with probability density W_{ab}^{MD} that is discussed in the following section. Altogether, the relative probability densities of displacement, deletion, and insertion trials are, respectively,

$$W_{ab}^0 = W^0 W_{ab}^{\text{MD}} \quad (10)$$

$$W_{ab}^{-i} = W^- W_a^{-i} W_{ab}^{\text{MD}} \quad (11)$$

$$W_{ab}^{+i} = W^+ W_a^{+i} W_{ab}^{\text{MD}}. \quad (12)$$

C. Generating trial states

Displacement, deletion, and insertion trials were generated using the trajectories of a Hamiltonian that combines real energies with fictitious momenta, \mathbf{p}^M , which are distinct from the physical values that were integrated out of the partition function. Most simply, $H(\mathbf{x}^M, \mathbf{p}^M) = \mathbf{p}^M \cdot \mathbf{p}^M / 2m + U(\mathbf{x}^M)$ for displacement trajectories. Each trial used the Verlet method to deterministically and reversibly integrate the system from some $(\mathbf{x}_a^M, \mathbf{p}_a^M)$ to $(\mathbf{x}_b^M, \mathbf{p}_b^M)$ over a fixed number of timesteps.

For a given \mathbf{x}_a^M , the choice of initial \mathbf{p}_a^M determines the final \mathbf{x}_b^M . Consequently, the probability density of a position trial, $W_{ab}^{\text{MD}}(\mathbf{x}_a^M, \mathbf{x}_b^M)$, can be related to the probability density of momenta selection, $W_a^{\text{MD}}(\mathbf{p}_a)$. More

specifically, integrating over final positions is equivalent to integrating over initial velocities [17],

$$\int d\mathbf{x}_b^M W_{ab}^{MD}(\mathbf{x}_a^M, \mathbf{x}_b^M) = \int d\mathbf{p}_a^M W_a^{MD}(\mathbf{p}_a^M), \quad (13)$$

which implies that $W_{ab}^{MD} = d\mathbf{p}_a^M/d\mathbf{x}_b^M W_a^{MD}$. Since the phase space of Hamiltonian dynamics is incompressible, Hamiltonian trajectories conserve the volume element, i.e. $d\mathbf{x}_b^M d\mathbf{p}_b^M = d\mathbf{x}_a^M d\mathbf{p}_a^M$. Therefore, the differentials cancel in Eq. (6) and can be neglected.

In all trials, the initial momenta were chosen to resemble those at the end of MD trajectories, which approach Maxwell-Boltzmann distributions. Every component was independently drawn with probability $\sqrt{\beta/2\pi m} e^{-\beta p^2/2m}$ such that the total relative probability was

$$W_{ab}^{MD}(\mathbf{x}_b^M) \propto W_a^{MD}(\mathbf{p}_a^M) \propto e^{-\beta \mathbf{p}_a^M \cdot \mathbf{p}_a^M/2m}. \quad (14)$$

If the next momenta were drawn equal to $-\mathbf{p}_b^M$, then the trajectory would run backwards, recovering \mathbf{x}_a^M . Therefore, the probability density of a reverse trial, $W_{ba}^{MD} = d\mathbf{p}_b^M/d\mathbf{x}_a^M W_b^{MD}(\mathbf{p}_b^M)$, is calculated by replacing \mathbf{p}_a^M with $-\mathbf{p}_b^M$ in Eq. (14).

D. Insertions and deletions

In insertion and deletion moves, the number of real particles was incremented from N to $N \pm 1$ by evolving the system under the Hamiltonian

$$H_\lambda = (1 - \lambda)H(\mathbf{x}^{N \subset M}, \mathbf{p}^M) + \lambda H(\mathbf{x}^{N \pm 1 \subset M}, \mathbf{p}^M), \quad (15)$$

where $\lambda = (t - t_a)/(t_b - t_a)$. This type of trajectory also conserves density in phase space [21]. As the velocities of untransformed fictitious particles retain constant magnitude during MD trajectories, their contribution to kinetic energy can be neglected. Indeed, their positions at the end of a trajectory could be immediately computed.

If certain particles are easier to insert or delete than others, then randomly selecting particles can be highly inefficient. Instead, deletion trials were biased to select particles with high energies. Atoms with initial energies $U_i(\mathbf{x}_a^{N \subset M})$ were specifically selected with probability

$$W_a^{-i} = \frac{e^{\beta^- U_i(\mathbf{x}_a^{N \subset M})}}{\sum_i^N e^{\beta^- U_i(\mathbf{x}_a^{N \subset M})}}, \quad (16)$$

where β^- is an adjustable parameter. This distribution temperature controls the strength of the selection bias, which reverts to random in the limit of $\beta^- = 0$.

Insertions can be guided similarly. Even though fictitious particles experience no interactions, their hypothetical energies upon insertion, $U_i^+(\mathbf{x}_a^M)$, were calculated based on the positions of real atoms. In an insertion trial, fictitious particle i was selected with probability

$$W_a^{+i} = \frac{e^{-\beta^+ U_i^+(\mathbf{x}_a^M)}}{\sum_i^{M-N} e^{-\beta^+ U_i^+(\mathbf{x}_a^M)}}, \quad (17)$$

using a distinct adjustable bias temperature, β^+ .

E. Method overview

In summary, μVT MC was performed through the following procedure:

0. Overlay N real particles with a non-interacting gas of $M - N$ fictitious particles to create an M -particle ensemble.
1. With fixed probabilities, choose to trial displacement (W^0), deletion (W^-), or insertion (W^+).
2. (a) If deleting, select a real atom with biased probability $W^{-i} \propto e^{-\beta^- U_i}$.
(b) If inserting, select a fictitious particle with biased probability $W^{+i} \propto e^{\beta^+ U_i^+}$.
3. Assign random non-physical momentum to every particle with probability $W^{MD} \propto e^{-\beta p^2/2m}$.
4. Update particle positions using Hamiltonian trajectories to deterministically generate a trial state of fully real and fictitious particles.
5. Calculate the probability of a reverse trial and accept or reject per the Metropolis-Hasting criterion of Eq. (7). Return to 1.

F. Volume sampling

The same techniques can also simulate NPT or μPT ensembles [6–8] by adding volume trials to step 1, which proceed directly to step 5 without performing MD. Volume integration introduces a microstate probability factor of e^{PV} in addition to the implicit V in $d\mathbf{x}^M$, which can be factored into $V d\mathbf{s}^M$ using dimensionless scaled coordinates, \mathbf{s}^M . For simplicity, V was sampled independently from \mathbf{s}^M and N with constant probability across some accessible interval. Given microstate probability

$$\pi'(\mathbf{x}^M) = \pi'(\mathbf{s}^M, V) \propto \frac{V^N}{\Lambda^{3N}} e^{-\beta(U(\mathbf{s}^{N \subset M}, V) + PV - \mu N)}, \quad (18)$$

the acceptance rate is determined from Eq. (7) using

$$\frac{\pi'(\mathbf{s}^M, V_b)}{\pi'(\mathbf{s}^M, V_a)} = \left(\frac{V_b}{V_a}\right)^N e^{-\beta(U(\mathbf{s}^{N \subset M}, V_b) - U(\mathbf{s}^{N \subset M}, V_a) + P(V_b - V_a))} \quad (19)$$

and uniform $W_{ba}^V/W_{ab}^V = 1$.

G. Demonstration

To illustrate the μVT MC procedure, Fig. 1(a) depicts a model system of liquid Cu at 1400 K, a little above the

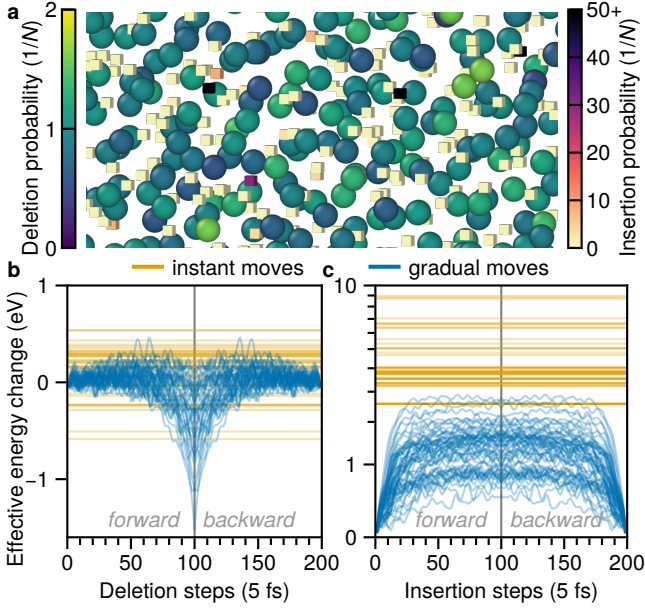


FIG. 1. Demonstration of μ VT MC calculations in a model system of liquid Cu at 1400 K. (a) Real atoms (spheres) are colored by deletion trial probabilities for a bias temperature of $4T$. Non-interacting fictitious particles (cubes) are colored by insertion trial probabilities for the same bias temperature. (b) Effective energy change during 100-step deletion attempts for randomly selected atoms. Equivalent values for instant moves without MD are drawn as horizontal lines for comparison. To illustrate essential reversibility, trials are run backwards by flipping velocities upon completion. (c) Similarly, the log-scale effective energy change during insertion trials, demonstrating the utility of gradual moves.

melting point, containing an equal number of real and fictitious particles. Density and chemical potential were equilibrium for $P = 0$ (see Methods for details). Real atoms are colored by their selection probability in a deletion trial with an arbitrarily chosen bias temperature of $4T$, or $\beta^- = \beta/4$. Fictitious particles are similarly colored by insertion probabilities for $\beta^+ = \beta/4$. While real energies are comparatively homogeneous, fictitious values vary greatly with only a few probable insertion options. Of course, selection probability distributions can be tuned by varying the bias temperature.

As a demonstration of gradual transformations, Fig. 1 also plots the effective energy change during 100-step (b) deletions and (c) insertions, which are compared to equivalent instant moves without MD (horizontal lines). The effective energy combines the potential energy of real, including transitional, particles and the kinetic energy, E_k , implied by their momenta. Though not physical, these momenta affect acceptance through the ratio $W_{ba}/W_{ab} \propto \exp(-\beta\Delta E_k)$ in Eq. (7). Effective energies also subtracted $-\mu\Delta N$ to account for the transforming particle. Gradual moves significantly reduced the energy barriers for both deletion and insertion. While deletions are still somewhat easier, the energy change must be

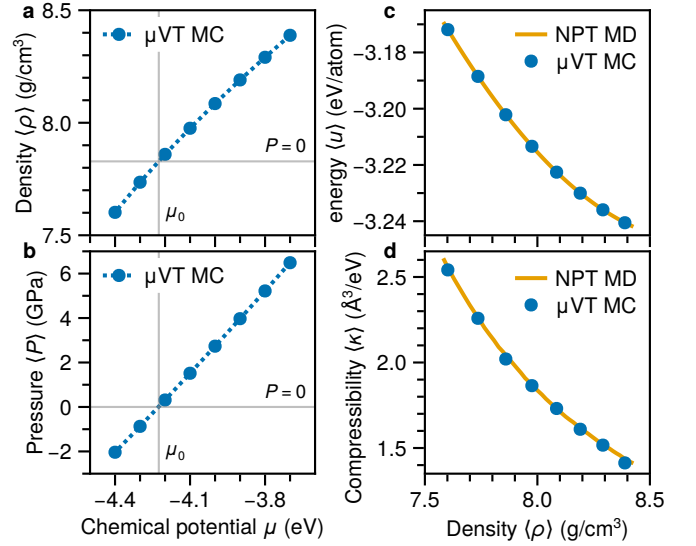


FIG. 2. Validation of μ VT MC calculations in the model system of 1400 K liquid Cu. Varying μ results in a range of (a) densities and (b) pressures. The chemical potential corresponding to zero pressure, μ_0 , provides the free energy of the homogeneous system. At all densities, μ VT calculations agree with NPT predictions for (c) potential energy per atom and (d) compressibility, which is calculated from density fluctuations.

significantly lower than in an insertion trial due to the inversion of prefactors between Eqs. (8) and (9). To demonstrate the reversibility required for detailed balance, velocities were flipped at the end of the 100-step trajectories, causing particles to move exactly backward.

H. Validation

The same system is also useful for validating the correctness of μ VT simulations as the liquid's homogeneity simplifies calculations of compressibility and free energy. Figure 2 reports properties at 8 different values of μ , which result in the densities shown in (a). The chemical potential corresponding to zero pressure in Fig. 2(b), $\mu \simeq -4.225$ eV, is the per-atom free energy of the homogeneous system. Figure 2(c) and (d) respectively show that μ VT MC consistently calculates the same energy per atom ($u = U/N$) and compressibility (κ) as NPT MD, with the latter confirming the correctness of number fluctuations (Eq. (23)). These calculations consistently reached an acceptance rate of at least 0.15 with relatively weak dependence on bias temperatures.

I. Optimization

Solids, however, can benefit from more careful optimization of simulation parameters, which were investigated in a simple fcc Cu crystal. Temperature was set to

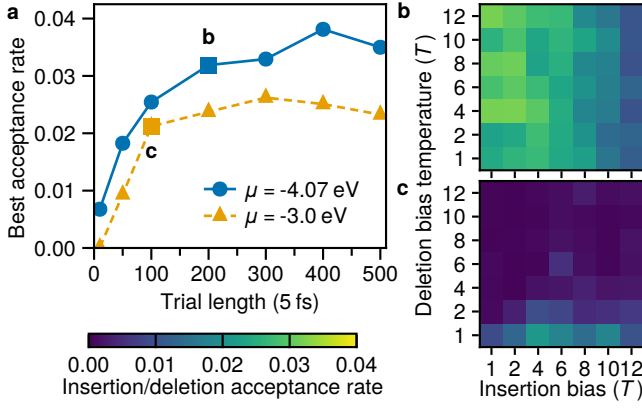


FIG. 3. Optimization of μVT simulation parameters in fcc Cu at 1200 K with equilibrium (-4.07 eV) and elevated (-3.0 eV) chemical potentials. (a) The maximum acceptance rate for insertions and deletions found by varying bias temperatures between T and $12T$ for different trajectory lengths. (b) Acceptance rate for each combination of bias temperatures for 200-step moves with $\mu = -4.07$ eV. (c) The same for 100-step moves with $\mu = -3.0$ eV. While deletion-controlled equilibrium simulations appear relatively flexible, insertion-limited calculations greatly benefit from specific parameter combinations.

1200 K so that simulations with the chemical potential of an equilibrium bulk crystal, $\mu = -4.07$ eV, contained a non-negligible concentration of vacancies. An elevated value of $\mu = -3.0$ eV was also considered to introduce a significant number of interstitials. In both scenarios, the number of MD steps in insertion and deletion trials was varied between 10 and 500. For each value, the insertion and deletion bias temperatures were independently varied from T to $12T$ to identify the combination providing the optimal acceptance rate, which is plotted in Fig. 3(a).

Acceptance probabilities below 0.05 are less than ideal but still allow for practical calculations. For simulations with $\mu = -4.07$ eV, the accepted moves primarily consisted of entropically expected deletions that were later filled by energetically favorable insertions. In this case, very short and even instant moves achieved finite acceptance rates that could offer better efficiency depending on computational overhead. However, this scenario is not generally representative of open systems, especially at higher pressures or chemical potentials. For the example of fcc Cu, Fig. 3(a) shows that simulations with $\mu = -3.0$ eV accepted essentially zero 10-step insertion or deletion trials.

Interestingly, Fig. 3(b) indicates that when acceptances were limited by the rate of deletion ($\mu = -4.07$ eV), a wide range of biasing parameters produced similar acceptance rates. When simulations were limited by the rate of insertion ($\mu = -3.0$ eV), however, Fig. 3(c) finds that viable acceptance rates required a deletion bias of 1 and insertion bias in the vicinity of 5. This scheme was used in the remaining calculations, for which it also

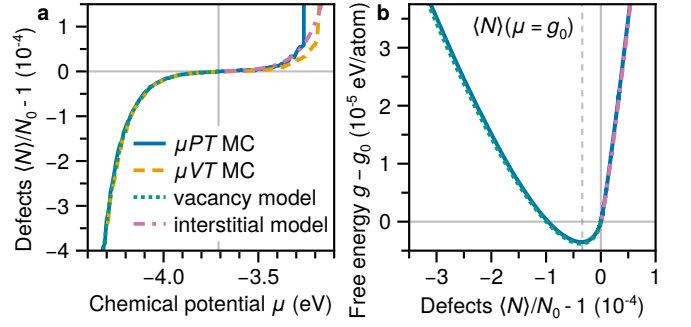


FIG. 4. μVT and μPT MC simulations of fcc Cu at 1200 K. (a) Interstitial or vacancy concentrations, represented in terms of excess atoms per site, $\langle N \rangle / N_0 - 1$, as a function of chemical potential. μPT calculations were fit to the analytical model represented by Eq. (21). (b) Gibbs free energy per atom from integrating $dG = \mu dN$ with reference to the Frenkel-Ladd free energy at N_0 . The free energy of the model is given by Eq. (20). The dashed line validates the approximation of $\mu \simeq g_0$ for calculating vacancy concentration in canonical equilibrium.

proved comparatively effective.

J. Point defects

With these optimizations, gradual transformations can effectively sample number degrees of freedom in solids. Continuing with the example of 1200 K fcc Cu, Fig. 4(a) plots the equilibrium number of atoms, which is measured in terms of interstitial or vacancy defects, across a range of chemical potentials in both μVT and μPT calculations. Defect concentration is specifically defined as $N/N_0 - 1$, where N_0 is the number of sites. While the crystal remains stable with a large number of vacancies, interstitials led to the formation of a new crystal plane corresponding to a sharp jump in $\langle N \rangle$, which could occur at a lower interstitial concentration in μPT simulations.

This data enables the determination of the complete free energy of a solid with point defects. The Helmholtz (F), and hence Gibbs ($G = F + PV$), free energies of a solid can be straightforwardly calculated by integration from a reference Einstein crystal [22, 23], but this approach fails at high temperatures when defects begin to diffuse. Free energies can be more accurately integrated from low-temperatures [24] or modeled with ideal configurational entropy [25], but both approaches requires the assumption of a specific defect configuration, e.g. a single monovacancy or divacancy. While large-scale calculations with free surfaces can form arbitrary defect states [26], they do not provide free energies. For μPT simulations of a given lattice, the observation that $\mu = (\partial G / \partial N)_{T,P}$ motivates an alternative approach of integrating $G(N) = G_0 + \int_{N_0}^N \mu dN'$ within the region of stability.

In reality, a crystal exposed to vacuum will minimize

its Gibbs free energy by forming internal defects, which grow or shrink the lattice while conserving the total number of atoms. For a μPT simulation representing part of an extended NPT crystal, this condition is equivalent to minimizing $g = G/N$. Using numerically integrated G , Fig. 4(b) plots g against $\langle N \rangle/N_0 - 1$ to reveal a minimum corresponding to the equilibrium vacancy concentration of an extended NPT crystal. In contrast to fluids, this is the only point where $\mu = g$ in a solid with point defects [27]. However, Fig. 4(b) indicates that the absolute difference between minimum g and g_0 is small enough that the extended NPT crystal can be approximated using $\mu \simeq g_0$. As validation, the vertical line in Fig. 4(b) indicates that $\langle N \rangle(\mu = g_0)$ coincides with the minimum in g within the resolution of the simulations.

The μPT calculations, which are exact in principle, can be further analyzed by comparison to a simple theoretical model. A perfect crystal with N_0 sites has an ideal free energy of $g_0 N_0$. The addition of $N_v = N_0 - N$ non-interacting vacancies contributes an ideal configurational entropy of $k_B \log \binom{N_0}{N_v}$. For a small number of vacancies under zero pressure, the change in free energy per vacancy can be approximated as $g_v - g_0$ for some g_v . With these simplifications,

$$G = N g_0 + N_v g_v - k_B T \left[N \log \left(\frac{N_v}{N} \right) - N_0 \log \left(\frac{N_v}{N_0} \right) \right]. \quad (20)$$

Taking $\mu = (\partial G / \partial N)_{T,P}$ and rearranging terms provides the vacancy concentration,

$$\frac{N}{N_0} = \frac{1}{1 + e^{-(\mu - g_0 + g_v)/k_B T}}. \quad (21)$$

Given g_0 , a value of g_v can be extracted from a single calculation of $N(\mu)$; from $\mu = -4.07$ eV, $g_v = 1.053$ eV. While interstitials can occupy additional sites, the same exercise implies an interstitial formation free energy of $g_i = 1.890$ eV at $\mu = -3.5$ eV. Using these values, Fig. 4(a) and (b) plot $\langle N \rangle$ and g according to the model given by Eqs. (20) and (21). The theory works very well as long as the lattice remains unchanged, which is not surprising given the low concentrations of point defects.

K. Interfaces

μPT MC is especially valuable for studying complex, extended defects such as crystal grain boundaries. Atomistic GBs are usually created by joining two misoriented crystals, but this construction does not generally correspond to physical equilibrium. Crucially, the structure of a given boundary will change as atoms are added or removed from its core. GBs form distinct phases at different atomic densities, which are usually represented as the fraction of an atomic plane parallel to the interface. The symmetric tilt and twist GBs considered in this study have only one such plane, which contains N_{\parallel} atoms in the area of a simulation. Since GB structure is unaffected by

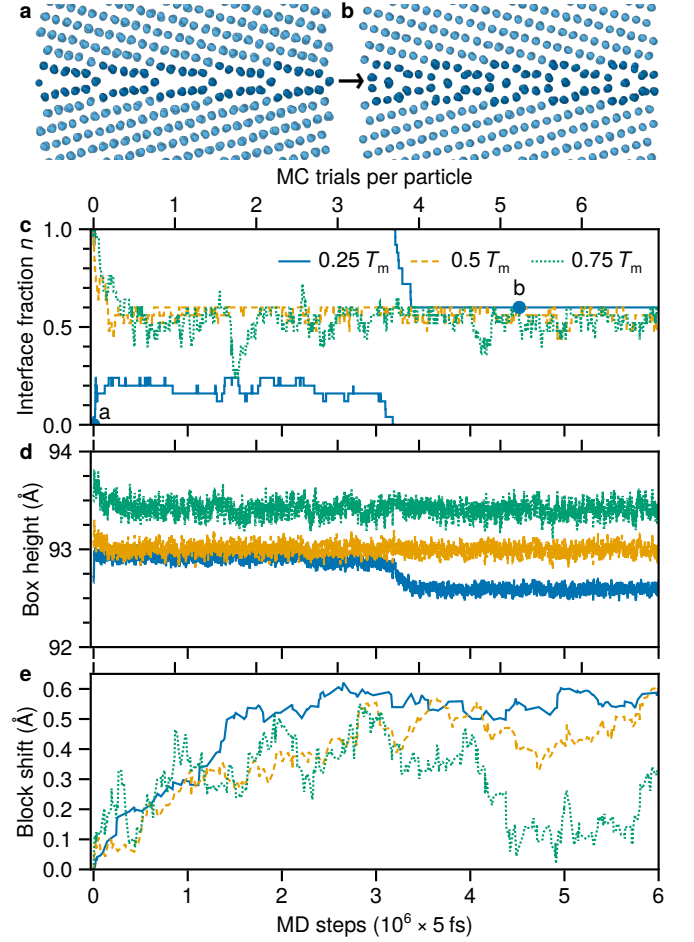


FIG. 5. μPT MC equilibration of a $\Sigma 27(552)(1\bar{1}0)$ tilt GB in W at 3 temperatures. (a) The initial structure, a 5×5 tiling of the periodic unit, is a bicrystal with integer (552) interface planes, i.e. $n = 0$. (b) The equilibrated structure at $T = 0.25 T_m$, which is slightly lower energy than previous optimizations. (c) Evolution of n vs. the number of MC trials or MD steps. (d) Similarly, the cell length normal to the boundary, which defines volume, due to normal displacements of the upper bounding block. (e) Displacement of the bounding block parallel to the boundary.

the addition or removal of an entire crystal plane parallel to the boundary, the atomic density is represented as

$$n = (N \bmod N_{\parallel}) / N_{\parallel}. \quad (22)$$

A general definition of n that includes asymmetric boundaries is given elsewhere [28].

Conventional NPT simulations with periodic boundary conditions artificially constrain n , preventing any GB transformations. This commonly employed approach often creates unphysical GBs such as amorphous phases at unphysically low temperatures [3, 4]. Without methods for open ensembles, rigorous studies of GB structure have largely focused on exploring 0 K ground states with different numbers of atoms [29–31]. These methods have proven successful for compositionally simple systems, but

cannot account for vibrational or configurational entropy, which affect interfaces as much as bulk phases. At high temperatures, open surface boundary conditions can allow atoms to diffuse in and out of a GB, but this approach requires large areas to mitigate surface effects and long simulation times that are limited by the rate of diffusion. μPT MC overcomes all of these limitations by exchanging particles with a reservoir representing an equilibrium bulk crystal. As discussed in the previous section, the crystal's chemical potential can be accurately approximated as the Gibbs free energy per atom, which was calculated using the Frenkel-Ladd method.

Since interface volume is not known *a priori*, the dimension perpendicular to the interface must also vary according to the pressure of the crystal. However, the periodic dimensions along the boundary should be fixed according to the bulk lattice parameter to prevent contraction from GB stress. As in previous studies [31, 32], the interface region was bounded with rigid crystalline blocks that defined the thermodynamic volume and elastically reflected encroaching particles. Depending on its position, \mathbf{r}_b , a bounding block contributes an additional potential energy term of $U_b(\mathbf{r}_b, \mathbf{x}^{N \leq M})$, which adds $U_b(\mathbf{x}^{N \leq M})$ to the Hamiltonian of trial trajectories. Volume moves were attempted by randomly displacing the upper block along the boundary normal within a range of uniform probability while scaling the coordinates of non-block particles. In order to account for variations in relative grain translations, additional MC trials similarly displaced the upper block parallel to the interface plane.

The following sections demonstrate the capabilities of μPT MC by application to W and Cu GBs with complex atomic structures that have been carefully studied by previous investigations. These GBs cannot be predicted with conventional techniques as they require optimization of the atomic density, exhibit large-area reconstructions, and feature intricate atomic arrangements that deviate significantly from simple constructions based on coincidence site lattices.

L. W grain boundary example

The $\Sigma 27(552)[1\bar{1}0]$ W GB provides an intriguing example of a non-trivial interface structure. For the interatomic potential of Ref. [33], a genetic algorithm predicted many distinct but nearly degenerate ground states corresponding to a 2×3 tiling of the periodic unit with $n = 0.5$, which could reflect aperiodicity [34]. Figure 5 describes μPT simulations of this GB, starting from the $n = 0$ construction depicted in (a), which is a 5×5 tiling of the periodic unit. Simulations at a quarter, half, and three-quarters of the experimental melting temperature ($T_m = 3695$ K) all quickly converged to the equilibrium $n = 0.6$ structure shown in Fig. 5(b) via the paths drawn in (c). Equilibration of the bounding block simultaneously led to a reduction in volume, which is plotted in

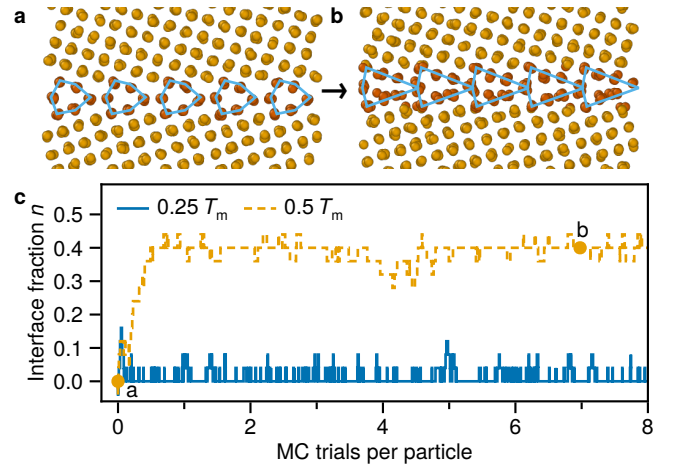


FIG. 6. μPT MC equilibration of a $\Sigma 5(310)[001]$ tilt GB in Cu at 3 temperatures. (a) The initial “normal kite” structure, a 5×5 tiling of the periodic unit, is the 0 K ground state with $n = 0$. (b) The equilibrated “split-kite” structure at $0.5 T_m$ has $n = 0.4$, in agreement with previous predictions. (c) Evolution of n during simulations, showing the metastability of the original phase at $0.25 T_m$.

(d), and a consistent translation parallel to the interface, which is shown in (e). The $n = 0.6$ structure appears very similar to the previously identified $n = 0.5$ ground states, but has about half a percent lower surface energy when relaxed at 0 K. The improvement is likely attributable to the ability of MC simulations to efficiently explore a larger, more flexible simulation cell.

M. Cu grain boundary example

μPT MC can also equilibrate GBs with finite-temperature phases that differ from the 0 K ground state. According to the interatomic potential of Ref. [35], a $\Sigma 5(310)[001]$ Cu tilt boundary exhibits a first-order phase transition from an $n = 0$ “kite” phase to an $n = 0.4$ “split-kite” phase at 180 K due to vibrational stabilization [32]. Figure 6 shows how μPT MC simulations at $0.5 T_m$ ($T_m = 1358$ K) transform $n = 0$ kites, which are depicted in Fig. 6(a), to the expected $n = 0.4$ split kites shown in (b), successfully capturing the phase transition. However, the original $n = 0$ kite structure remains stable at $0.25 T_m$, albeit with notable fluctuations toward $n = 0.4$.

N. Controlling the chemical potential

The two previous examples considered chemical potentials representing equilibrium bulk crystals, but phenomena such as creep, rapid quenching, or radiation damage may lead to non-equilibrium defect concentrations corresponding to different chemical potentials. μPT simu-

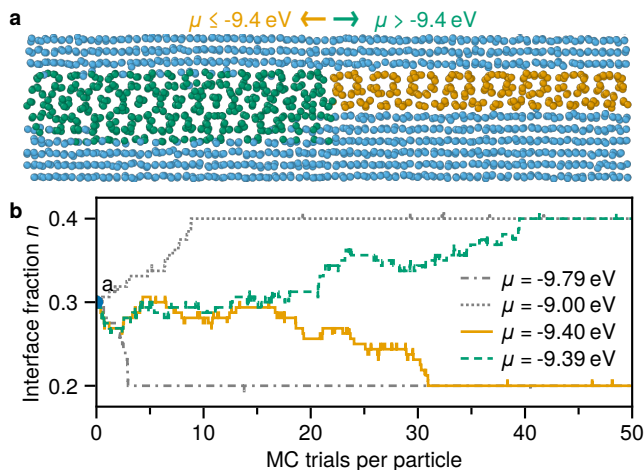


FIG. 7. μPT MC equilibration of different structures in a W $\Sigma 5(001)(310)$ twist GB by varying the chemical potential at $T = 0.5 T_m$. (a) To overcome large nucleation barriers, the initial structure contains both the equilibrium $n = 0.2$ phase (right, yellow) and a higher-energy $n = 0.4$ phase (left, green). (b) Evolution of n for a range of chemical potentials; the transition point is between $\mu = -9.40$ eV and $\mu = -9.39$ eV.

lations can also model how these conditions cause GBs to transform. Most interface transitions exhibit significant hysteresis due to nucleation barriers [36], but the coexistence point of two GB phases can be identified by systematically varying the chemical potential.

For example, Fig. 7(a) depicts a $\Sigma 5(100)(310)$ -twist boundary containing an $n = 0.2$ ground state (right) and a distinct $n = 0.4$ phase (left) that is metastable under ambient conditions. This configuration corresponds to equilibrium coexistence in NPT simulations, but determining its chemical potential requires an open ensemble. Figure 7(b) plots the evolution of n in μPT simulations beginning from the depicted two-phase structure for several different μ . At the value corresponding to an equilibrium crystal ($\mu = -9.788$ eV), the ground state rapidly grows to eclipse the metastable phase. For significantly elevated chemical potentials (e.g. $\mu = -9.0$ eV), the $n = 0.4$ phase similarly replaces the ground state. Kinetics become increasingly sluggish near the transition point, which, despite low acceptance rates, is shown to lie between $\mu = -9.4$ and -9.39 eV.

III. DISCUSSION AND CONCLUSION

Low insertion and deletion acceptance rates may partially reflect the physical rarity of these defects, but can still likely be increased. For instance, the criteria for successful acceptance could be explicitly learned from descriptors representing the local volume or atomic environment. Preferentially aligning initial velocities with forces around transformed particles could also potentially aid relaxations. As another possibility, fictitious par-

ticles could actively move towards low-energy sites under unidirectional forces, though introducing such interactions would require significant changes to the underlying formalism. Yet even with single-digit acceptance rates, practical simulations, such as interface structure determination, appear computationally affordable and remain accessible with larger interface areas and orders-of-magnitude more expensive interatomic potentials.

The other main limitation of the MC framework is the size-dependent accumulation of numerical error during MD trajectories, which eventually prevents the acceptance of both displacement and number moves. Simulations with 5 fs timesteps are limited to $\sim 10^5$ atoms, though smaller timesteps allow many-times larger cells. Still some kind of parallelization scheme across local partitions [37] seems necessary to simulate systems above a certain size. Insertions and deletions could particularly benefit from reduced numerical error in localized trajectories and, in contrast to canonical moves, inherently require parallelization to scale with system size.

Opportunities for improvement notwithstanding, the method enables practical simulations of solid systems that are altogether inaccessible with conventional methods. This success ultimately depends on two key components. First, the introduction of fictitious particles sets up a biasing scheme that greatly improves sampling efficiency over random insertions and deletions. Gradually transforming these particles through MD trajectories then enables moves—especially insertions—that would be otherwise impossible. μVT and μPT simulations using these techniques demonstrate particular promise for studying crystals defects, especially GBs. The approach can be easily extended to simulate interfaces in alloys, which inherently require finite-temperature simulations to describe ordering and are generally too complex for exhaustive ground-state explorations. These simulations would likely benefit from the addition of chemical swaps to complement insertions and deletions, perhaps through a similar gradual mechanism.

IV. METHODS

All simulations were performed using the LAMMPS code [38] with a new “fix” that will be detailed in a future publication. Structures were rendered with Ovito [39] and plots were made using Makie [40].

Simulations of liquid Cu began with 2048 real atoms and an equal number of fictitious particles in a $30 \times 30 \times 30$ Å periodic cell with $T = 1400$ K and $\mu = -4.228$ eV. Interactions were modeled using the embedded-atom method (EAM) potential of Ref. [35]. Prior to the demonstration of gradual moves, randomly distributed particles were equilibrated by trialing 10^4 100-step displacement trajectories with 5 fs timesteps. 100 insertions or deletions were then trialed (and subsequently reversed) with 0.5 probability each, with specific particles chosen using a bias temperature of $4T$.

Validation calculations were performed similarly, with the addition of 50-step displacement trials that were attempted with equal probability. After equilibration over $5 \cdot 10^6$ trials, simulations ran for $8 \cdot 10^7$ trials to sample fluctuations. Reference *NPT* MD simulations ran for $5 \cdot 10^8$ 1 fs steps using a Nosé-Hoover thermostat and barostat [41]. Compressibility [42] was calculated either as

$$\kappa_{\mu VT} = \frac{V}{k_B T} \frac{\langle N^2 \rangle - \langle N \rangle^2}{\langle N \rangle^2} \quad (23)$$

or

$$\kappa_{NPT} = \frac{1}{k_B T} \frac{\langle V^2 \rangle - \langle V \rangle^2}{\langle V \rangle}. \quad (24)$$

Simulations of solid Cu began with 4000 fictitious particles and 4000 real atoms in a $10 \times 10 \times 10$ conventional fcc lattice, which was equilibrated at 1200 K under 0 pressure using the same interatomic potential. Insertion/deletion acceptance rates were then estimated by trialing, on average, 10^4 insertions or deletions and an equal number of 50-step displacement trajectories, all with 5 fs timesteps.

Defect concentrations were similarly calculated by attempting 100-step insertions or deletions, with respective temperature bias factors of 5 and 1, and 50-step canonical moves with equal probability over 10^7 MD steps. Chemical potential was incremented by 0.01 eV and numerically integrated from the ideal free energy of $f_0 = f(n=0) = -4.07$ eV/atom, which was calculated using the Frenkel-Ladd method [22, 23].

The W $\Sigma 27(552)(1\bar{1}0)$ tilt boundary was modeled as a 5×5 tiling of the unit cell created by joining crystals sections defined by $[1\bar{1}0]$, $[\frac{1}{2}\frac{1}{2}\frac{5}{2}]$, and $2[5,5,2]$. After relaxing the initial bicrystal, real particles were randomly displaced by 0.2 \AA to ease MC thermalization. 50-step canonical moves were trialed with 0.7 probability using 5 fs timesteps. 200-step insertions and deletions were trialed with 0.1 probability each and respective bias factors of 5 and 1. Upper block displacements with magnitude up to 0.1 \AA were trialed both in- and out-of-plane, each with 0.05 probability and 0 pressure. Simulations employed the EAM potential of Ref. [33], which was used to calculate equilibrium temperature/lattice parameter/chemical potential combina-

tions of 924 K/ 3.1644 \AA /-9.2318 eV, 1848 K/ 3.1768 \AA /-9.8799 eV, and 2771 K/ 3.1928 \AA /-10.6655 eV.

The Cu $\Sigma 5(310)[001]$ tilt boundary was similarly modeled using a unit cell created by joining crystal sections defined by $[001]$, $[\frac{1}{2}\frac{3}{2}0]$, and $8[\frac{3}{2}\frac{1}{2}0]$. The $n = 1$ normal-kite phase was then canonically equilibrated using 2000 50-step trials with 5 fs timesteps. μPT simulations began from a 5×5 tiling of this structure and used the same parameters as before. Using the EAM potential of Ref. [35], temperature/lattice parameter/chemical potential combinations were 340 K/ 3.6345 \AA /-3.5758 eV, 679 K/ 3.6565 \AA /-3.7352 eV, and 1019 K/ 3.6786 \AA /-3.9445 eV.

In order to accommodate two initial phases, the W $\Sigma 5(001)[310]$ twist boundary was constructed as an 8×2 tiling of the unit cell created by joining crystal sections defined by $[310]$, $[\bar{1}30]$, and $14[001]$. Simulations were performed at 1848 K using the EAM potential of Ref. [43] with a lattice parameter of 3.1909 \AA . After removing 0.6 of the interface plane from one half of the cell and 0.8 from the other, the two phases formed over $2 \cdot 10^5$ 50-step displacement trials, using 5 fs timesteps, during which block displacements up to 0.1 \AA were attempted with 0.1 probability both in- and out-of-plane. Subsequent μVT calculations were performed as before, but with 2 fs timesteps due to the larger system size and low rate of acceptance.

ACKNOWLEDGMENTS

T. Oppelstrup is thanked for helpful discussions. This work was performed under the auspices of the U.S. Department of Energy by Lawrence Livermore National Laboratory under Contract DE-AC52-07NA27344. The project was supported by the U.S. Department of Energy, Office of Science under an Office of Fusion Energy Science Early Career Award and partly supported by the LLNL Laboratory Directed Research and Development (LDRD) program under project tracking code 22-SI-007. Computational resources were provided by the LLNL Institutional Computing Grand Challenge program and the Oak Ridge Leadership Computing Facility at the Oak Ridge National Laboratory, which is supported by the U.S. Department of Energy, Office of Science under Contract No. DE-AC05-00OR22725.

-
- [1] P. W. Tasker and D. M. Duffy, On the structure of twist grain boundaries in ionic oxides, *Phil. Mag. A* **47**, L45 (1983).
 - [2] S. R. Phillpot and J. M. Rickman, Simulated quenching to the zero-temperature limit of the grand-canonical ensemble, *J. Chem. Phys.* **97**, 2651 (1992).
 - [3] S. von Althan, P. D. Haynes, K. Kaski, and A. P. Sutton, Are the Structures of Twist Grain Boundaries in Silicon Ordered at 0 K?, *Phys. Rev. Lett.* **96**, 055505 (2006).

- [4] T. Frolov, D. L. Olmsted, M. Asta, and Y. Mishin, Structural phase transformations in metallic grain boundaries, *Nat. Commun.* **4**, 1899 (2013).
- [5] T. Frolov, S. V. Divinski, M. Asta, and Y. Mishin, Effect of Interface Phase Transformations on Diffusion and Segregation in High-Angle Grain Boundaries, *Phys. Rev. Lett.* **110**, 255502 (2013).
- [6] T. L. Hill, Thermodynamics of Small Systems, *J. Chem. Phys.* **36**, 3182 (1962).

- [7] U. Marzolino, μPT statistical ensemble: systems with fluctuating energy, particle number, and volume, *Sci. Rep.* **11**, 15096 (2021).
- [8] A. Campa, L. Casetti, I. Latella, Agustín Pérez-Madrid, and S. Ruffo, Concavity, Response Functions and Replica Energy, *Entropy* **20**, 907 (2018).
- [9] D. Tanguy, Sampling vacancy configurations with large relaxations using Smart Darting, *Phys. Rev. Mater.* **8**, 033604 (2024).
- [10] T. Çağın and B. M. Pettitt, Grand Molecular Dynamics: A Method for Open Systems, *Molecular Simul.* **6**, 5 (1991).
- [11] T. Çağın and B. M. Pettitt, Molecular dynamics with a variable number of molecules, *Molecular Phys.* **72**, 169 (1991).
- [12] S. Boinepalli and P. Attard, Grand canonical molecular dynamics, *J. Chem. Phys.* **119**, 12769 (2003).
- [13] H. Eslami and F. Müller-Plathe, Molecular dynamics simulation in the grand canonical ensemble, *J. Comput. Chem.* **28**, 1763 (2007).
- [14] W. Shi and E. J. Maginn, Continuous Fractional Component Monte Carlo: An Adaptive Biasing Method for Open System Atomistic Simulations, *J. Chem. Theory Comput.* **3**, 1451 (2007).
- [15] A. Rahbari, R. Hens, M. Ramdin, O. A. Moulton, D. Dubbeldam, and T. J. H. Vlugt, Recent advances in the continuous fractional component Monte Carlo methodology, *Molecular Simul.* **47**, 804 (2021).
- [16] S. Duane, A. D. Kennedy, B. J. Pendleton, and D. Roweth, Hybrid Monte Carlo, *Phys. Lett. B* **195**, 216 (1987).
- [17] B. Mehlig, D. W. Heermann, and B. M. Forrest, Hybrid Monte Carlo method for condensed-matter systems, *Phys. Rev. B* **45**, 679 (1992).
- [18] L. Belloni, Non-equilibrium hybrid insertion/extraction through the 4th dimension in grand-canonical simulation, *J. Chem. Phys.* **151**, (2019).
- [19] J. Kim, L. Belloni, and B. Rotenberg, Grand-canonical molecular dynamics simulations powered by a hybrid 4D nonequilibrium MD/MC method: Implementation in LAMMPS and applications to electrolyte solutions, *J. Chem. Phys.* **159**, 12769 (2023).
- [20] L. A. Rowley, D. Nicholson, and N. G. Parsonage, Monte Carlo grand canonical ensemble calculation in a gas-liquid transition region for 12-6 Argon, *J. Comput. Phys.* **17**, 401 (1975).
- [21] C. Jarzynski, Nonequilibrium Equality for Free Energy Differences, *Phys. Rev. Lett.* **78**, 2690 (1997).
- [22] D. Frenkel and A. J. C. Ladd, New Monte Carlo method to compute the free energy of arbitrary solids. Application to the fcc and hcp phases of hard spheres, *J. Chem. Phys.* **81**, 3188 (1984).
- [23] R. Freitas, M. Asta, and M. de Koning, Nonequilibrium free-energy calculation of solids using LAMMPS, *Comput. Mater. Sci.* **112**, 333 (2016).
- [24] S. M. Foiles, Evaluation of harmonic methods for calculating the free energy of defects in solids, *Phys. Rev. B* **49**, 14930 (1994).
- [25] X. Zhang, B. Grabowski, T. Hickel, and Jörg Neugebauer, Calculating free energies of point defects from *ab initio*, *Comput. Mater. Sci.* **148**, 249 (2018).
- [26] M. I. Mendelev and Y. Mishin, Molecular dynamics study of self-diffusion in bcc Fe, *Phys. Rev. B* **80**, 144111 (2009).
- [27] W. W. Mullins and R. F. Sekerka, On the thermodynamics of crystalline solids, *J. Chem. Phys.* **82**, 5192 (1985).
- [28] I. S. Winter and T. Frolov, Quantifying and visualizing the microscopic degrees of freedom of grain boundaries in the Wigner–Seitz cell of the displacement-shift-complete lattice, *Acta Mater.* **291**, 120968 (2025).
- [29] Q. Zhu, A. Samanta, B. Li, R. E. Rudd, and T. Frolov, Predicting phase behavior of grain boundaries with evolutionary search and machine learning, *Nat. Commun.* **9**, 467 (2018).
- [30] A. D. Banadaki, M. A. Tschoopp, and S. Patala, An efficient Monte Carlo algorithm for determining the minimum energy structures of metallic grain boundaries, *Comput. Mater. Sci.* **155**, 466 (2018).
- [31] E. Chen, T. W. Heo, B. C. Wood, M. Asta, and T. Frolov, Grand canonically optimized grain boundary phases in hexagonal close-packed titanium, *Nat. Commun.* **15**, 7049 (2024).
- [32] R. Freitas, R. E. Rudd, M. Asta, and T. Frolov, Free energy of grain boundary phases: Atomistic calculations for $\Sigma 5(310)[001]$ grain boundary in Cu, *Phys. Rev. Mater.* **2**, 093603 (2018).
- [33] M.-C. Marinica, L. Ventelon, M. R. Gilbert, L. Provaille, S. L. Dudarev, J. Marian, G. Bencteux, and F. Willaime, Interatomic potentials for modelling radiation defects and dislocations in tungsten, *J. Phys. Condens. Matter* **25**, 395502 (2013).
- [34] T. Frolov, W. Setyawan, R. J. Kurtz, J. Marian, A. R. Oganov, R. E. Rudd, and Q. Zhu, Grain boundary phases in bcc metals, *Nanoscale* **10**, 8253 (2018).
- [35] Y. Mishin, M. J. Mehl, D. A. Papaconstantopoulos, A. F. Voter, and J. D. Kress, Structural stability and lattice defects in copper: *Ab initio*, tight-binding, and embedded-atom calculations, *Phys. Rev. B* **63**, 224106 (2001).
- [36] I. S. Winter, R. E. Rudd, T. Oppelstrup, and T. Frolov, Nucleation of Grain Boundary Phases, *Phys. Rev. Lett.* **128**, 035701 (2022).
- [37] B. Sadigh, P. Erhart, A. Stukowski, A. Caro, E. Martinez, and L. Zepeda-Ruiz, Scalable parallel Monte Carlo algorithm for atomistic simulations of precipitation in alloys, *Phys. Rev. B* **85**, 184203 (2012).
- [38] A. P. Thompson, H. M. Aktulga, R. Berger, D. S. Bolintineanu, W. M. Brown, P. S. Crozier, P. J. in 't Veld, A. Kohlmeyer, S. G. Moore, T. D. Nguyen, R. Shan, M. J. Stevens, J. Tranchida, C. Trott, and S. J. Plimpton, LAMMPS - a flexible simulation tool for particle-based materials modeling at the atomic, meso, and continuum scales, *Comput. Phys. Commun.* **271**, 108171 (2022).
- [39] A. Stukowski, Visualization and analysis of atomistic simulation data with OVITO—the Open Visualization Tool, *Modelling Simul. Mater. Sci. Eng.* **18**, 015012 (2010).
- [40] S. Danisch and J. Krumbiegel, Makie.jl: Flexible high-performance data visualization for Julia, *J. Open Source Softw.* **6**, 3349 (2021).
- [41] W. Shinoda, M. Shiga, and M. Mikami, Rapid estimation of elastic constants by molecular dynamics simulation under constant stress, *Phys. Rev. B* **69**, 134103 (2004).
- [42] T. L. Hill, *Statistical Mechanics* (McGraw-Hill, New York, 1956).
- [43] X. W. Zhou, R. A. Johnson, and H. N. G. Wadley, Misfit-energy-increasing dislocations in vapor-deposited CoFe/NiFe multilayers, *Phys. Rev. B* **69**, 144113 (2004).